GEOPHYSICS, VOL. 72, NO. 2 (MARCH-APRIL 2007); P. WA85–WA95, 14 FIGS., 5 TABLES.
10.1190/1.2435082

Special Section — Marine Controlled-Source Electromagnetic Methods

A Bayesian model for gas saturation estimation using marine seismic AVA and CSEM data

Jinsong Chen[1], G. Michael Hoversten[1], Donald Vasco[1], Yoram Rubin[2], and Zhangshuan Hou[2]

ABSTRACT

We develop a Bayesian model to jointly invert marine seismic amplitude versus angle (AVA) and controlled-source electromagnetic (CSEM) data for a layered reservoir model. We consider the porosity and fluid saturation of each layer in the reservoir, the bulk and shear moduli and density of each layer not in the reservoir, and the electrical conductivity of the overburden and bedrock as random variables. We also consider prestack seismic AVA data in a selected time window as well as real and quadrature components of the recorded electrical field as data. Using Markov chain Monte Carlo (MCMC) sampling methods, we draw a large number of samples from the joint posterior distribution function. With these samples, we obtain not only the estimates of each unknown variable, but also various types of uncertainty information associated with the estimation. This method is applied to both synthetic and field data to investigate the combined use of seismic AVA and CSEM data for gas saturation estimation. Results show that the method is effective for joint inversion; the incorporation of CSEM data reduces uncertainty in fluid saturation estimation compared to inversion of seismic AVA data alone. The improvement in gas saturation estimation obtained from joint inversion for field data is less significant than for synthetic data because of the large number of unknown noise sources inherent in the field data.

INTRODUCTION

Estimating reservoir parameters for gas exploration from geophysical data is challenging and subject to a large degree of uncertainty. Seismic imaging techniques, such as seismic amplitude versus angle (AVA) analysis, can provide good information about the physical location and porosity of potential gas-bearing sands but cannot discriminate between economical and uneconomical gas concentrations. This is because seismic velocity and density have low sensitivity to variations in gas saturation (Castagna and Backus, 1993; Debski and Tarantola, 1995; Plessix and Bork, 2000). Controlled-source electromagnetic (CSEM) methods can discriminate between uneconomical and economical gas saturation because electrical resistivity of reservoir materials is highly sensitive to water saturation. However, estimating gas saturation using CSEM data alone is impractical because CSEM data have low spatial resolution.

Seismic AVA and CSEM methods are sensitive to different physical properties of reservoir materials. Seismic AVA data are functions of the seismic P- and S-wave velocity and density of reservoir materials. CSEM data are functions of the electrical resistivity of reservoir materials, the overburden, and the bedrock. Because both elastic and electrical properties of gas reservoirs are related physically to fluid saturation and porosity through rock-physics models (Archie, 1942; Gassmann, 1951; Mavko et al., 1998), joint inversion of seismic AVA and CSEM data has the potential to provide better estimates of gas saturation and porosity than inversion of individual data sets.

We consider a 1D (or layered) reservoir model in this study, where forward simulation of seismic AVA and CSEM data is quick. This is a simplified representation of a deepwater gas reservoir in the Gulf of Mexico, where the spatial variability of fluid saturation and porosity changes only along the vertical direction. We assume that rock-

Manuscript received by the Editor April 4, 2006; revised manuscript received September 19, 2006; published online March 1, 2007.
[1]Lawrence Berkeley National Laboratory, Earth Sciences Division, Berkeley, California. E-mail: jchen@lbl.gov; gmhoversten@lbl.gov; dwvasco@lbl.gov.
[2]University of California at Berkeley, Department of Civil and Environmental Engineering, Berkeley, California. E-mail: rubin@ce.berkeley.edu; huo@berkeley.edu.

physics models for linking the elastic and electrical properties to fluid saturation and porosity are obtainable from the nearby borehole logs; therefore, we ignore the effects of uncertainty in rock-physics models at this stage.

A deterministic inverse method and a minimum relative entropy (MRE) method for estimating gas saturation according to the same layered reservoir model using seismic AVA and CSEM data are given by Hoversten et al. (2006) and Hou et al. (2006), respectively. In this paper, we focus on the development of a Bayesian model and use Markov chain Monte Carlo (MCMC) methods to investigate the combined use of seismic AVA and CSEM data for fluid saturation and porosity estimation.

METHODOLOGY

Bayesian model

The Bayesian model is developed for an offshore gas exploration scenario, such as the Gulf of Mexico and the North Sea. As shown in Figure 1, we consider a layered reservoir model that may include gas, oil, and water. Seismic data are prestack common-midpoint (CMP) gathers containing several incident angles over a predefined time window that covers the reservoir. The time window is determined from check shots or sonic-log calculations of time-depth pairs. We estimate water and gas saturation and porosity within the reservoir, where oil saturation can be calculated from the water and gas saturation. We also estimate elastic bulk and shear moduli and density in the zones outside the reservoir because well logs necessary for deriving rock-physics models to link fluid saturation and porosity to seismic AVA data are typically only available within the reservoir.

Marine CSEM data are the real (in-phase) and quadrature (out-of-phase) components of the recorded electrical field from various receivers located on the seafloor for given sources with different frequencies. Those data are the responses to the electrical conductivity of the entire half-space, which includes the seawater, the overburden above the reservoir, the reservoir, and the bedrock beneath the reservoir. Because the electrical conductivities in the seawater and in the overburden and bedrock often affect the estimates of fluid saturation in the reservoir, we also consider them as unknown parameters in this model.

We assume in this study that the rock-physics models for linking reservoir fluid saturation and porosity to reservoir seismic velocity and density and the Archie's law for linking reservoir water saturation and porosity to reservoir electrical conductivity are given and

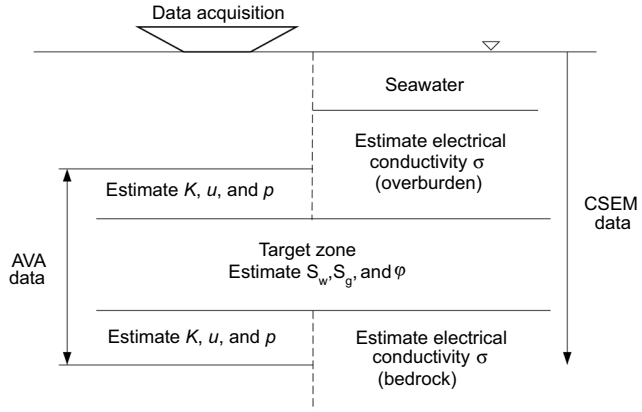

Figure 1. Schematic map of a layered reservoir model.

are exact. These assumptions can be relaxed to account for uncertainty in rock-physics models and Archie's law in other studies. Let vectors $\mathbf{S}_w$, $\mathbf{S}_g$, and $\boldsymbol{\varphi}$ denote reservoir water saturation, gas saturation, and porosity, respectively, which can be used to calculate reservoir seismic P- and S-wave velocity and density. Let vectors $\mathbf{K}$, $\boldsymbol{\mu}$, and $\boldsymbol{\rho}$ denote the bulk modulus, shear modulus, and density above and beneath the gas reservoir, respectively, which can be transformed into seismic P- and S-wave velocity and density in the layers outside the reservoir. Let matrix $\mathbf{R}$ represent seismic AVA data, which are explicit functions of seismic P- and S-wave velocity and density within and outside the reservoir and are implicit functions of reservoir parameters ($\mathbf{S}_w$, $\mathbf{S}_g$, and $\boldsymbol{\varphi}$) and elastic properties ($\mathbf{K}$, $\boldsymbol{\mu}$, and $\boldsymbol{\rho}$) in the zones outside the reservoir.

Let vector $\boldsymbol{\sigma}$ denote the electrical conductivity of the seawater, the overburden, and the bedrock. Let matrix $\mathbf{E}$ represent CSEM data, which are explicit functions of electrical conductivity, $\boldsymbol{\sigma}$ in the seawater, the overburden, and the bedrock and indirect functions of reservoir porosity $\boldsymbol{\varphi}$ and water saturation $\mathbf{S}_w$. Because seismic AVA and CSEM data are two different types of geophysical measurements, we assume that they are independent of each other. Consequently, we obtain the following Bayesian model:

$$\begin{aligned} f(\mathbf{S}_w,\mathbf{S}_g,\boldsymbol{\varphi},\boldsymbol{\sigma},\mathbf{K},\boldsymbol{\mu},\boldsymbol{\rho}|\mathbf{R},\mathbf{E}) \\ \propto f(\mathbf{R}|\mathbf{S}_w,\mathbf{S}_g,\boldsymbol{\varphi},\mathbf{K},\boldsymbol{\mu},\boldsymbol{\rho}) \\ f(\mathbf{E}|\mathbf{S}_w,\boldsymbol{\varphi},\boldsymbol{\sigma}) f(\mathbf{S}_w,\mathbf{S}_g,\boldsymbol{\varphi},\boldsymbol{\sigma},\mathbf{K},\boldsymbol{\mu},\boldsymbol{\rho}). \end{aligned} \quad (1)$$

Equation 1 defines a joint posterior probability distribution function of all unknown parameters, which is known up to a normalizing constant. The first term on the right side of the equation is the likelihood function of seismic AVA data, the second term on the right side is the likelihood function of CSEM data, and the last term on the right side is the prior distribution of all unknown variables.

Likelihood model

We determine the likelihood functions of seismic AVA and CSEM data based on their error structures in data acquisition and processing. Seismic AVA reflectivity is an explicit function of seismic P- and S-wave velocity and density in the reservoir and in the zones outside the reservoir. In our application, we use the Zoeppritz equations (Aki and Richards, 1980) to model the reflectivity. Seismic P- and S-wave velocity and density in the reservoir are calculated from water and gas saturation and porosity ($\mathbf{S}_w$, $\mathbf{S}_g$, and $\boldsymbol{\varphi}$) using rock-physics models. Seismic P- and S-wave velocity and density in the zones outside the reservoir are calculated from bulk and shear moduli and density ($\mathbf{K}$, $\boldsymbol{\mu}$, and $\boldsymbol{\rho}$). Let the seismic AVA data matrix be $\mathbf{R} = \{r_{ij}\}$, where $i = 1,2,\ldots, m_t$ (m_t is the number of time samples) and $j = 1,2,\ldots, m_a$ (m_a is the number of incident angles). Thus,

$$r_{ij} = M^a_{ij}(\mathbf{S}_w,\mathbf{S}_g,\boldsymbol{\varphi},\mathbf{K},\boldsymbol{\mu},\boldsymbol{\rho}) + \varepsilon^a_{ij}, \quad (2)$$

where M^a_{ij} is the ijth component of the seismic AVA forward model and ε^a_{ij} is the corresponding measurement error. Let $\boldsymbol{\varepsilon} = (\varepsilon^a_{11}, \varepsilon^a_{21},\ldots, \varepsilon^a_{m_t,1}, \varepsilon^a_{12}, \varepsilon^a_{22}\ldots, \varepsilon^a_{m_t,2},\ldots, \varepsilon^a_{m_t,m_a})^T$ be a vector representing all measurement errors, where T is the transpose of the vector. Let $n = m_a m_t$ be the total number of seismic data in a given time window. To consider correlation of those errors in time and across incident angles, we assume that they have the multivariate Gaussian distribution with zero mean and covariance matrix $\boldsymbol{\Sigma}$, as used by Buland and

Omre (2003a). Consequently, we obtain the likelihood function for the seismic data as follows:

$$f(\mathbf{R}|\mathbf{S_w},\mathbf{S_g},\boldsymbol{\varphi},\mathbf{K},\boldsymbol{\mu},\boldsymbol{\rho}) = \frac{1}{\sqrt{(2\pi)^n|\boldsymbol{\Sigma}|}}\exp\left(-\frac{1}{2}\boldsymbol{\varepsilon}^T\boldsymbol{\Sigma}^{-1}\boldsymbol{\varepsilon}\right), \quad (3)$$

where $|\boldsymbol{\Sigma}|$ and $\boldsymbol{\Sigma}^{-1}$ denote the determinant and the inverse of the covariance matrix, respectively. If the error structure is nonGaussian and can be modeled, other appropriate likelihood functions should be used.

Determining the likelihood function of CSEM data is more difficult than determining the likelihood function of seismic AVA data because the amplitudes of the recorded electrical field span several orders of magnitude. The CSEM data used in this study include real and quadrature components of the recorded electrical fields at various offsets for different frequencies. Let the CSEM data matrix be $\mathbf{E} = \{e_{ijk}\}$, where $i = 1,2,\ldots, n_f$ represent different frequencies of CSEM sources, $j = 1,2,\ldots, n_0$ represent different offsets, and $k = 1,2$ represent real and quadrature components of the recorded electrical field. Thus,

$$e_{ijk} = M^e_{ijk}(\mathbf{S_w},\boldsymbol{\varphi},\boldsymbol{\sigma}) + \varepsilon^e_{ijk}, \quad (4)$$

where M^e_{ijk} is the ijkth component of the CSEM forward model and ε^e_{ijk} is the corresponding measurement error. Unlike the seismic AVA data, we only consider uncorrelated noise in this study. We assume that the errors of CSEM data are proportional to their corresponding measurements with a random ratio ε^r_{ijk}, i.e., $\varepsilon^e_{ijk} = \varepsilon^r_{ijk}e_{ijk}$. We assume that the relative ratio ε^r_{ijk} has the Gaussian distribution with zero mean and standard deviation β_j that is given and may depend on offsets, typically increasing from near to far offsets, for example, from 5% to 10%. As a result, we obtain the following likelihood function:

$$f(\mathbf{E}|\mathbf{S_w},\boldsymbol{\varphi},\boldsymbol{\sigma}) = \prod_{i=1}^{n_f}\prod_{j=1}^{n_o}\prod_{k=1}^{2}\frac{1}{\sqrt{2\pi\beta_j^2}}\exp\left\{-\frac{1}{2\beta_j^2}\left(\frac{e_{ijk} - M^e_{ijk}(\mathbf{S_w},\boldsymbol{\varphi},\boldsymbol{\sigma})}{e_{ijk}}\right)^2\right\}. \quad (5)$$

Like the seismic AVA data, we should use other appropriate likelihood functions if the error structure of CSEM data is nonGaussian.

Prior model

The prior distribution is determined from prior knowledge and other information about the unknown parameters (such as nearby borehole data), which may be subjective and site specific. In this study, we assume that the unknown parameters in the reservoir (i.e., $\mathbf{S}_w$, $\mathbf{S}_g$, $\boldsymbol{\varphi}$) are independent of the variables in the layers outside the reservoir (i.e., $\boldsymbol{\sigma}$, $\mathbf{K}$, $\boldsymbol{\mu}$, $\boldsymbol{\rho}$) and water and gas saturation $\mathbf{S}_w$, $\mathbf{S}_g$ are independent of porosity $\boldsymbol{\varphi}$. We also assume that the electrical conductivity $\boldsymbol{\sigma}$ in the thick overburden and bedrock is independent of the elastic bulk and shear moduli and density ($\mathbf{K},\boldsymbol{\mu},\boldsymbol{\rho}$) in the thin layers above and beneath the reservoir, and the bulk and shear moduli and density ($\mathbf{K},\boldsymbol{\mu},\boldsymbol{\rho}$) are independent of each other. Consequently, we simplify the prior distribution function as

$$f(\mathbf{S_w},\mathbf{S_g},\boldsymbol{\varphi},\boldsymbol{\sigma},\mathbf{K},\boldsymbol{\mu},\boldsymbol{\rho}) = f(\mathbf{S_w},\mathbf{S_g})f(\boldsymbol{\varphi})f(\boldsymbol{\sigma})f(\mathbf{K})f(\boldsymbol{\mu})f(\boldsymbol{\rho}). \quad (6)$$

The prior distribution functions of water and gas saturation are determined jointly because gas and water saturation are dependent. Let (a_1,b_1), (a_2,b_2), and (a_3,b_3) be the prior bounds of water, gas, and oil saturation. As shown in Figure 2, the inversion domain of water and gas saturation is a joint set given by

$$D = \{(S_w,S_g): S_w \in (a_1,b_1), S_g \in (a_2,b_2), S_o \in (a_3,b_3), S_w + S_g + S_o = 1\}. \quad (7)$$

We assume that the prior distribution of water and gas saturation is uniform on the domain D. For all other parameters, we assume that their prior distributions are uniform within their corresponding given ranges.

SAMPLING METHODS

We use sampling methods to estimate unknown parameters from the joint posterior distribution function shown in equation 1. Ordinary Monte Carlo methods are impracticable for this application because of the high dimensionality of unknown variables; therefore, we use MCMC sampling methods. MCMC methods have been shown to be useful for inverting complex geophysical data by Bosch (1999), Malinverno (2002), and Buland and Omre (2003b, c).

Unlike ordinary Monte Carlo methods that draw independent random samples directly from the joint distribution, MCMC methods draw samples by running elaborately constructed Markov chains for a long time (Gilks et al., 1996). The constructed Markov chains are stationary and have the joint posterior distribution as the limit distribution. In addition, the chains are ergodic under weak conditions (i.e., irreducible and aperiodic).

According to the ergodic theorem (Gelfand and Smith, 1990), the sample mean of any measurable function of those unknown variables asymptotically converges to its corresponding true expectation as the number of runs is sufficiently large. The commonly used measurable functions are the mean, variance, and mode of the unknown variables. An important function is the probability of any particular event concerning unknown variables. Indeed, a major strength of MCMC methods is the ability to focus directly on the estimates of probabilities (such as marginal probabilities or probability density

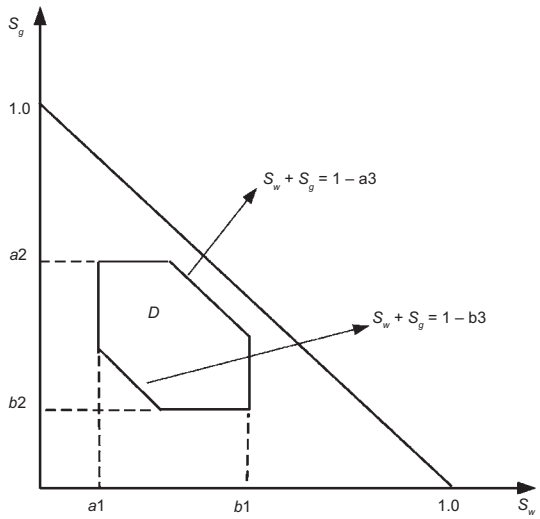

Figure 2. Inversion domain of water and gas saturation defined by given water, gas, and oil saturation bounds [i.e., $S_w \in (a_1,b_1)$, $S_g \in (a_2,b_2)$, and $S_o \in (a_3,b_3)$].

functions of unknown variables), in contrast to the more indirect calculation via moment approximations and asymptotic limit theorems (Besag, 2001).

Many methods are available to construct Markov chains, for example, Gibbs sampler (Geman and Geman, 1984), Metropolis-Hastings methods (Metropolis et al., 1953; Hastings, 1970), and slice sampling methods (Neal, 2003). In this study, we combine Metropolis-Hastings methods with slice sampling methods to obtain samples of unknown parameters. For water and gas saturation, we use multivariate Metropolis-Hastings methods; for all other unknowns ($\boldsymbol{\varphi}$, $\boldsymbol{\sigma}$, $\mathbf{K}$, $\boldsymbol{\mu}$, $\boldsymbol{\rho}$) we use mixing sampling methods that include both Metropolis-Hastings and slice sampling methods. In the following, we first briefly outline the general steps of our MCMC sampling; the details are given later.

We draw samples using MCMC methods by sequentially updating unknown vectors $\mathbf{S}_w$, $\mathbf{S}_g$, $\boldsymbol{\varphi}$, $\boldsymbol{\sigma}$, $\mathbf{K}$, $\boldsymbol{\mu}$, $\boldsymbol{\rho}$ with the following four steps:

1) Assign initial values to get $\mathbf{S}_w^{(0)}, \mathbf{S}_g^{(0)}, \boldsymbol{\varphi}^{(0)}, \boldsymbol{\sigma}^{(0)}, \mathbf{K}^{(0)}, \boldsymbol{\mu}^{(0)}, \boldsymbol{\rho}^{(0)}$, and let $t = 0$.
2) Update water and gas saturation ($\mathbf{S}_w$, $\mathbf{S}_g$) given ($\mathbf{S}_w^{(t)}$, $\mathbf{S}_g^{(t)}$, $\boldsymbol{\varphi}^{(t)}$, $\boldsymbol{\sigma}^{(t)}$, $\mathbf{K}^{(t)}$, $\boldsymbol{\mu}^{(t)}$, $\boldsymbol{\rho}^{(t)}$) using the multivariate Metropolis-Hastings method to get ($\mathbf{S}_w^{(t+1)}, \mathbf{S}_g^{(t+1)}$).
3) Update porosity $\boldsymbol{\varphi}$, conductivity $\boldsymbol{\sigma}$, bulk and shear moduli, and density $\mathbf{K}$, $\boldsymbol{\mu}$, $\boldsymbol{\rho}$ given $\mathbf{S}_w^{(t+1)}$, $\mathbf{S}_g^{(t+1)}$, $\boldsymbol{\varphi}^{(t)}$, $\boldsymbol{\sigma}^{(t)}$, $\mathbf{K}^{(t)}$, $\boldsymbol{\mu}^{(t)}$, $\boldsymbol{\rho}^{(t)}$, using mixing sampling methods that include Metropolis-Hastings and slice sampling methods to get ($\boldsymbol{\varphi}^{(t+1)}$, $\boldsymbol{\sigma}^{(t+1)}$, $\mathbf{K}^{(t+1)}$, $\boldsymbol{\mu}^{(t+1)}$, $\boldsymbol{\rho}^{(t+1)}$).
4) Repeat steps 2 and 3 until the allowed maximum number of runs is reached.

Metropolis-Hastings sampling methods

Because of dependence between water and gas saturation, we use a multivariate Metropolis-Hastings method to draw samples of water and gas saturation ($\mathbf{S}_w$, $\mathbf{S}_g$). We first derive the conditional distribution of ($\mathbf{S}_w$, $\mathbf{S}_g$) given all other variables. For simplicity, we denote it as $f(\mathbf{S}_w,\mathbf{S}_g|\cdot)$, where the dot represents all other variables. This conditional distribution function is proportional to the joint posterior distribution function shown on the left side of equation 1. By retaining only those terms that are related to water and gas saturation, we obtain the following conditional probability distribution function:

$$f(\mathbf{S}_w,\mathbf{S}_g|\cdot) \propto f(\mathbf{R}|\mathbf{S}_w,\mathbf{S}_g,\boldsymbol{\varphi},\mathbf{K},\boldsymbol{\mu},\boldsymbol{\rho})f(\mathbf{E}|\mathbf{S}_w,\boldsymbol{\varphi},\boldsymbol{\sigma})f(\mathbf{S}_w,\mathbf{S}_g). \tag{8}$$

As shown in equation 7 and Figure 2, we assume that the prior distribution of water and gas saturation in each layer is uniform on the domain D. Therefore, we can drop the prior distribution $f(\mathbf{S}_w,\mathbf{S}_g)$ from equation 8 to further simplify the conditional distribution function.

We can use various proposal distributions to draw candidate samples of water and gas saturation. In this study, we use the uniform distribution defined on D as the proposal distribution. In this case, the probability α for accepting a candidate sample is equal to its likelihood ratio, as shown in equation 9. Suppose the current values of water and gas saturation are ($\mathbf{S}_w^{(t)},\mathbf{S}_g^{(t)}$), which certainly is a vector in D as shown in Figure 2. We want to obtain a new vector of water and gas saturation ($\mathbf{S}_w^{(t+1)},\mathbf{S}_g^{(t+1)}$).

There are four steps in the procedure. First, we generate a candidate vector ($\mathbf{S}_w^*,\mathbf{S}_g^*$) uniformly from D as shown in Figure 2. Second, we calculate the probability for accepting the candidate vector:

$$\alpha = \min\left(1, \frac{f(\mathbf{R}|\mathbf{S}_w^*,\mathbf{S}_g^*,\boldsymbol{\varphi}^{(k)},\mathbf{K}^{(t)},\boldsymbol{\mu}^{(t)},\boldsymbol{\rho}^{(t)})}{f(\mathbf{R}|\mathbf{S}_w^{(t)},\mathbf{S}_g^{(t)},\boldsymbol{\varphi}^{(t)},\mathbf{K}^{(t)},\boldsymbol{\mu}^{(t)},\boldsymbol{\rho}^{(t)})} \cdot \frac{f(\mathbf{E}|\mathbf{S}_w^*,\boldsymbol{\varphi}^{(t)},\boldsymbol{\sigma}^{(t)})}{f(\mathbf{E}|\mathbf{S}_w^{(t)},\boldsymbol{\varphi}^{(t)},\boldsymbol{\sigma}^{(t)})}\right). \tag{9}$$

Third, we generate a random value u uniformly from interval $(0,1)$. Fourth, if $u < \alpha$, let $\mathbf{S}_w^{(t+1)} = \mathbf{S}_w^*$ and $\mathbf{S}_g^{(t+1)} = \mathbf{S}_g^*$; otherwise, let $\mathbf{S}_w^{(t+1)} = \mathbf{S}_w^{(t)}$ and $\mathbf{S}_g^{(t+1)} = \mathbf{S}_g^{(t)}$.

By repeating steps 1–4, we obtain many samples of water and gas saturation $\{(\mathbf{S}_w^{(t)},\mathbf{S}_g^{(t)}):t = 0,1,2,\ldots\}$. From the procedure we see that the vector ($\mathbf{S}_w^{(t+1)},\mathbf{S}_g^{(t+1)}$) depends solely on the vector ($\mathbf{S}_w^{(t)},\mathbf{S}_g^{(t)}$), not on the vectors $\{(\mathbf{S}_w^{(r)},\mathbf{S}_g^{(r)}):r \le t-1\}$.

Slice sampling methods

We use slice sampling methods described by Neal (2003) and Metropolis-Hastings methods to obtain samples of porosity $\boldsymbol{\varphi}$, overburden and bedrock conductivity $\boldsymbol{\sigma}$, bulk modulus $\mathbf{K}$, shear modulus $\boldsymbol{\mu}$, and density $\boldsymbol{\rho}$ from the joint posterior distribution given in equation 1. This is because sampling efficiency for the Metropolis-Hastings methods is very sensitive to the choice of tuning parameters, but slice sampling methods are less so. In fact, for this application, we are unable to set good values for Metropolis-Hastings methods to generate Markov chains that converge at a sufficient speed. Because the slice sampling methods for obtaining samples of porosity, electrical conductivity, bulk and shear moduli, and density are similar, we briefly describe the single-variable slice sampling methods for updating porosity.

We first derive the conditional distribution function of porosity $\boldsymbol{\varphi}$ given all other variables from equation 1. Similar to water and gas saturation, by retaining only those terms that are related to porosity, we obtain the following conditional:

$$f(\boldsymbol{\varphi}|\cdot) \propto f(\mathbf{R}|\mathbf{S}_w,\mathbf{S}_g,\boldsymbol{\varphi},\mathbf{K},\boldsymbol{\mu},\boldsymbol{\rho})f(\mathbf{E}|\mathbf{S}_w,\boldsymbol{\varphi},\boldsymbol{\sigma})f(\boldsymbol{\varphi}). \tag{10}$$

Let φ_i be the porosity in a given layer i. We assume that the prior distribution of the porosity is uniform on interval (c,d), where c and d denote the lower and upper bounds of the porosity. We work on the logarithmic porosity as used by Bosch (2004). Let variable x be the transformation of porosity φ_i defined on $(-\infty, +\infty)$ and given by $x = \log((\varphi_i - c)/(d - \varphi_i))$. The Jacobian of φ_i at x is given by $J = e^x/((d-c)(1+e^x)^2)$. The conditional distribution of the transformed porosity given all other variables thus can be written as

$$\begin{aligned} f(x|\cdot) &= |J|f(\varphi_i|\cdot) \\ &\propto \frac{e^x}{(1+e^x)^2} f(\mathbf{R}|\mathbf{S}_w,\mathbf{S}_g,\boldsymbol{\varphi},\mathbf{K},\boldsymbol{\mu},\boldsymbol{\rho})f(\mathbf{E}|\mathbf{S}_w,\boldsymbol{\varphi},\boldsymbol{\sigma})f(\boldsymbol{\varphi}). \end{aligned} \tag{11}$$

Notice that all bold symbols on the right side of equation 11 represent vectors, and the vector $\boldsymbol{\varphi}$ includes component φ_i and therefore is a function of x. To simplify the description, we let $\pi(x) = f(x|\cdot)$, which is a probability density function (PDF) of x. Our goal is to draw samples from this PDF using slice sampling methods. Figure 3 shows an example of using the single-variable slice sampling method given by Neal (2003) to obtain a new value x_1 from the current value x_0. First, we draw a value y, which is uniformly distributed on $(0, \pi(x_0))$. The value y defines a horizontal slice, $S = \{x: y < \pi(x)\}$, shown as thick lines in Figure 3. Note that x_0 is always within S. Sec-

ond, we find an interval, $I = (L,R)$, near the value x_0 that contains all or most of the slice, where L and R represent the lower and upper bounds of the interval. Third, we draw a new value x_1 from the part of the slice within the interval.

Steps 2 and 3 can be implemented in several ways. In this study, we use a stepping-out method to find the interval I and a shrinkage method to draw a new value from the interval. We step out in both directions from the value x_0 with a given interval width for a given maximum number of iterations until both ends are outside the slice. We then uniformly pick a new value from the interval. If the value picked is inside the slice, we consider it as the new value x_1; otherwise, we use the value to shrink the interval. Neal (2003) shows how this procedure guarantees that the obtained chains converge to PDF $\pi(x)$.

Strategies for speeding convergence

The success of MCMC methods depends on the efficiency of the sampling methods used. If a sampling method is inefficient, we may need to run a very long chain; thus, the computational effort is very large. Typically, the raw sampling methods (for both Metropolis-Hastings and slice sampling methods) are not efficient. We need to tune the parameters that control chain movements. Unfortunately, the efficiency of a sampling method is often problem specific.

In this study, we use a multivariate Metropolis-Hastings method to obtain samples of water and gas saturation, but a mixing method to obtain samples of other variables. At each sampling step, we randomly pick one of the following four methods: single-variable Metropolis-Hastings methods, multivariate Metropolis-Hastings methods, single-variable slice sampling methods, or multivariate slice sampling methods. This strategy has been shown to be efficient for solving our joint inversion problems.

SYNTHETIC EXAMPLE

The following synthetic case study is designed to show the capability and flexibility of our joint inversion approach for integrating different types of information and to demonstrate the benefits of joint inversion of marine seismic AVA and CSEM data for gas saturation estimation.

Synthetic true model

The synthetic reservoir includes five layers with a thickness of 30 m and zero oil saturation. From the upper to the bottom layers, the gas saturation of the reservoir is 0.05, 0.95, 0.4, 0.9, and 0.1, and porosity is 0.15, 0.25, 0.15, 0.1, and 0.05, respectively. Above the gas reservoir is the overburden with a thickness of 1400 m and electrical conductivity of 1.0 S/m. Above the overburden is 1000 m of seawater with conductivity of 3.2 S/m. The bedrock beneath the reservoir has electrical conductivity of 1.0 S/m. To account for uncertainty in selecting a suitable time window for seismic AVA data inversion, we add one 30-m-thick layer above the reservoir and one 30-m-thick layer below the reservoir, and we invert for elastic bulk and shear moduli and density in those layers.

Rock-physics model

The rock-physics model used in the synthetic and field studies for linking reservoir porosity and fluid saturation to seismic P- and S-wave velocity and density is described in detail by Dvorkin and Nur (1996) and Hoversten et al. (2003). This model uses the Hertz-Mindlin contact theory (Mindlin, 1949) for dry frame bulk and shear moduli of a dense, random pack of spherical grains. The modified Hashin-Shtrikman lower bound (Hashin and Shtrikman, 1963) is used to calculate the effective moduli for porosity below the critical porosity. The bulk modulus of fluid-saturated rock is calculated by Gassmann's equation (Gassmann, 1951), and the bulk moduli and density of brine, oil, and gas are computed using the relations from Batzle and Wang (1992). The reservoir electrical conductivity is calculated using Archie's law (Archie, 1942) from reservoir porosity and water saturation. Tables 1 and 2 list the specific parameters used in this study that are obtained by fitting the rock-physics model and Archie's law to the well logs collected from the Troll site in North Sea by Hoversten et al. (2006).

Synthetic data

The seismic AVA data are NMO-corrected angle gathers generated by convolving a 28 Hz Ricker wavelet with the angle-dependent reflectivity for each layer interface, sampled at 2 ms for six incident angles (5°, 10°, 15°, 20°, 25°, and 30°). The seismic velocity and density outside of the reservoir are calculated directly from bulk and shear moduli and density. The seismic velocity and density in the reservoir are calculated from porosity and fluid saturation using the rock-physics model parameters given in Table 1. The Zoeppritz equations (Aki and Richards, 1980) are used to calculate the angle-dependent reflectivity. We assume that the synthetic seismic data include spatially correlated Gaussian random noise and the spatial correlation is determined by the exponential variogram with an integral length of 6 ms. The variance of the Gaussian noise is angle dependent and the signal-to-noise ratios are 10, 9, 8, 7, 6, and 5 from the near to the far offsets.

Synthetic EM data simulate commercial EM field data collected using CSEM techniques. The marine CSEM system consists of a ship-towed electric dipole source and a number of seafloor-deployed recording instruments capable of recording orthogonal electric (and optionally magnetic) fields. A common configuration consists of an electric dipole transmitter, 100–300 m in length, towed in a neutrally buoyant configuration approximately 50 m off the seafloor to avoid collision with stationary receiver systems (Ellingsrud et al.,

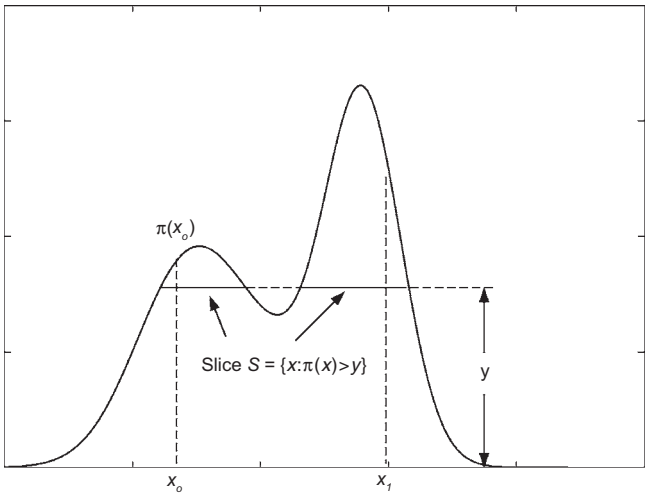

Figure 3. An example using a single-variable slice sampling method to update a Markov chain from the current value x_0 to the new value x_1.

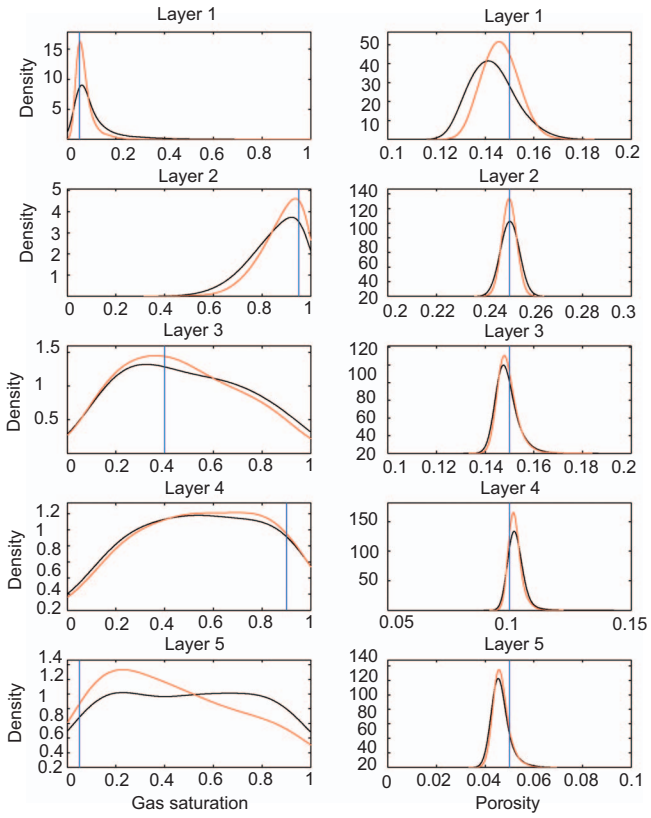

Figure 4. A comparison between the estimated PDFs of gas saturation and porosity using seismic AVA data with signal-to-noise ratios from 10 to 5 (black) and from 20 to 10 (red). The vertical straight lines show the true values.

Table 1. Rock-physics model parameters derived from data collected from well 31/2–1.

Parameters	Values
Critical porosity	0.38
Number of grain contacts	13.50
Grain shear modulus (Gpa)	22.50
Grain Poisson's ratio	0.34
Grain density (kg/m^3)	2567.00
Oil API gravity	28.50
Brine salinity	0.07
Gas gravity	0.59
Temperature (°C)	65.00

Table 2. Archie's law coefficients obtained using data collected from well 31/2–1.

Parameters	Fitted values
Archie's law constant	0.78
Water saturation exponent	−1.31
Porosity exponent	−0.14

2002). A square wave of electric current is sent into the transmitter at a variable fundamental frequency between 0.1 and 10 Hz. The earth response, along with the primary field from the transmitter, is measured at the array of receivers. In this study, we use CSEM sources with five frequencies (0.10, 0.25, 0.50, 0.75, and 1.00 Hz) and eight source-receiver offsets (2, 3, 4, 5, 6, 7, 8, and 10 km). The relationship between reservoir electrical resistivity and reservoir porosity and water saturation is given by Archie's law using coefficients listed in Table 2. We add 5%–10% relative Gaussian random noise to the synthetic CSEM data from the near to the far offsets.

Inversion using seismic AVA data alone

We first demonstrate the capability of the stochastic model to distinguish high-gas-saturation layers from low-gas-saturation layers using seismic AVA data alone. We consider two levels of noise that correspond to S/N from 10 to 5 and from 20 to 10 from near to far offsets. We assume that oil saturation is zero in each layer, the unknown parameters in equation 1 are porosity and gas saturation in the five layers, and the bulk and shear moduli and density outside of the reservoir. We also assume that the prior distribution of gas saturation is uniform on (0, 1) and the prior distribution of porosity is uniform on (0, 0.35).

Figure 4 shows the estimated PDFs of gas saturation and porosity using seismic AVA data only. The black and red curves are the marginal PDFs of gas saturation and porosity in the five layers using the seismic AVA data with S/N from 10 to 5 and from 20 to 10, respectively; the blue straight lines are their corresponding true values. The figure shows that the seismic data provide (1) good estimates of porosity in each layer, (2) good estimates of gas saturation in layers 1 and 2, but (3) poor estimates of gas saturation in layers 3, 4, and 5. With the decrease of seismic noise, uncertainty in gas saturation and porosity decreases. Table 3 shows the rms of the estimated values using seismic data with S/N from 10 to 5 and from 20 to 10. The comparison between the true values and the estimated means, medians, and modes shows that the improvement in accuracy for both gas saturation and porosity is small even when the signal-to-noise ratios of seismic data are increased by a factor of two.

Inversion using both seismic AVA and CSEM data

We next demonstrate the benefits of joint inversion of seismic AVA and CSEM data for gas saturation estimation. We assume that the synthetic CSEM data have relative errors linearly increasing from 5% at the nearest offset to 10% at the furthest offset. Figure 5 compares the estimated PDFs of gas saturation and porosity using only seismic AVA data, with S/N from 10 to 5 (black), and with the estimates derived using both seismic AVA and CSEM data (red).

Table 3. The rms errors of the estimated values using seismic AVA data with signal-to-noise ratios from 10 to 5 and from 20 to 10.

	Signal-to-noise ratios	Estimated mean	Estimated median	Estimated mode
Gas saturation	10 to 5	0.2709	0.2689	0.1723
	20 to 10	0.2366	0.2180	0.0641
Porosity	10 to 5	0.0037	0.0038	0.0039
	20 to 10	0.0025	0.0025	0.0026

Joint inversion of seismic AVA and CSEM data reduces uncertainty in gas saturation estimation, especially for layers 4 and 5. With the joint inversion, we are able to identify two high-gas-concentration layers (2 and 4) and two low-gas-concentration layers (1 and 5) by the major modes of their corresponding PDFs. Table 4 shows the rms errors of the estimated values using both seismic and electromagnetic (EM) data. The incorporation of CSEM data improves the estimates of both gas saturation and porosity. The improvement in gas saturation estimation is significant.

Effects of unknown overburden and bedrock electrical conductivity

We explore the effects of uncertainty in the overburden and bedrock electrical conductivity by assuming the overburden and bedrock conductivities are unknown and are uniformly distributed on given ranges. We consider uncertainty ranges of 10% and 30% about their true values. Figure 6 compares the estimated PDFs of gas saturation and porosity by assuming the overburden and bedrock conductivity is given (black), has 10% uncertainty (red), and has 30% uncertainty (blue). Uncertainty in the overburden and bedrock conductivity has limited effects on the estimated PDFs of gas saturation and porosity. In each case, the major modes of the estimated PDFs are close to their true values. The uncertainty associated with the estimation generally increases as the prior bounds of the overburden and bedrock conductivity increase, but the increase is not significant. This is possibly because CSEM data in the synthetic model can provide good information on the overburden and bedrock conductivity.

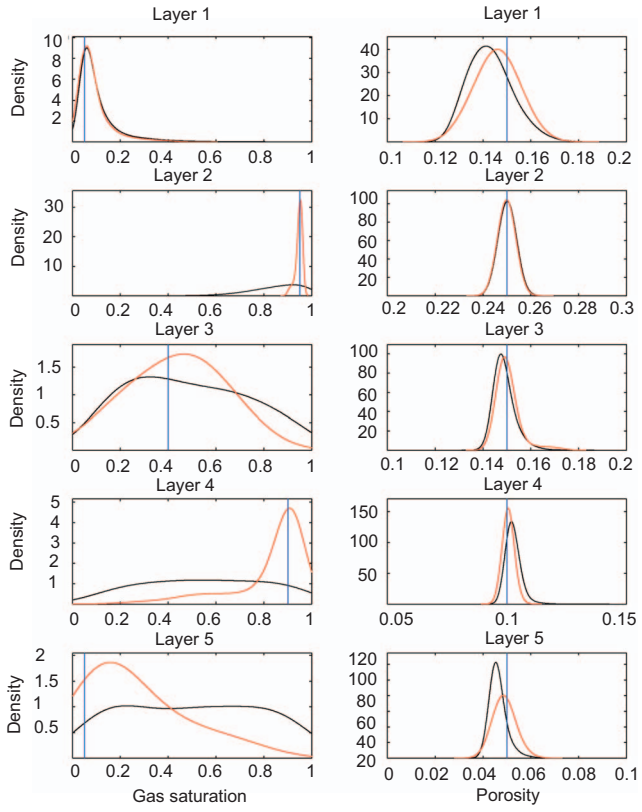

Figure 5. A comparison between the estimated PDFs of gas saturation and porosity obtained from inversion of seismic AVA data alone (black) and from inversion of both seismic AVA and CSEM data (red).

Effects of unknown oil concentration

In the preceding inversion, we assume that oil saturation in the reservoir is zero. In reality, however, oil saturation in each layer may be another parameter that needs to be estimated. To investigate the effects of our prior knowledge about the oil saturation on joint inversion, we assume that oil saturation lies in the ranges of (0, 0.1) and (0, 0.3). Although the true oil saturation remains zero in all layers, we allow oil saturation to take values between the above ranges when we invert seismic AVA and CSEM data.

Figure 7 compares the estimated PDFs of gas saturation and porosity obtained from joint inversion by assuming that the oil saturation is equal to zero (black), uniformly distributed on (0, 0.1) (red), and uniformly distributed on (0, 0.3) (blue). The unknown oil saturation has little effect on the estimates of porosity but has significant effect on estimates of gas saturation. For example, for layers 2 and 4 with increasing uncertainty in the unknown oil concentration, the estimated PDFs of gas saturation are biased toward the lower values.

Table 4. The rms errors of the estimated values using seismic AVA data with signal-to-noise ratios from 10 to 5 and CSEM data with relative errors from 5% to 10%.

	Estimated mean	Estimated median	Estimated mode
Gas saturation	0.0839	0.0373	0.0336
Porosity	0.0019	0.0018	0.0017

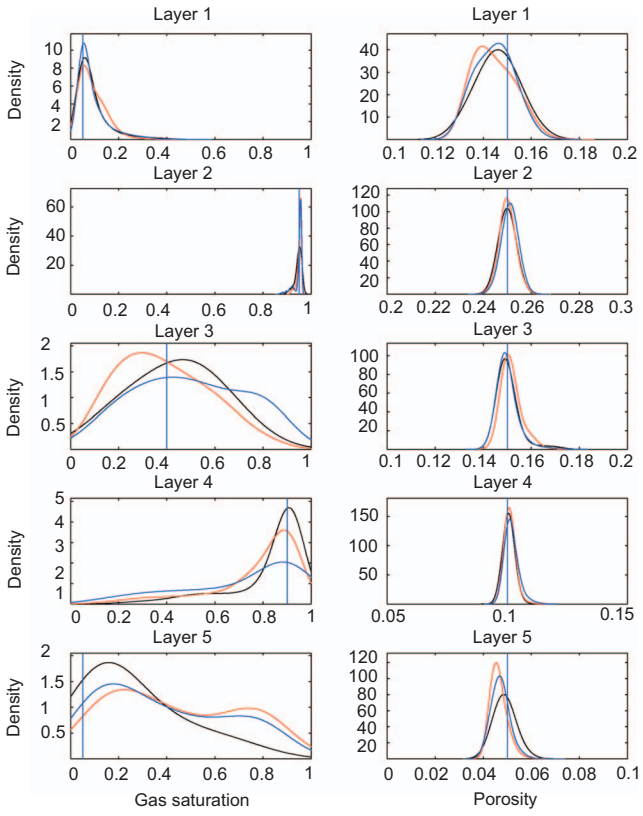

Figure 6. A comparison between the estimated PDFs of gas saturation and porosity obtained from joint inversion by assuming the overburden and bedrock conductivity is given (black), and has 10% (red) and 30% (blue) uncertainty around the true values.

FIELD EXAMPLE

In this section, we apply the Bayesian model to field data obtained from the Troll site in the North Sea. We compare the estimates of gas and oil saturation with the measurements at a nearby borehole to evaluate the benefits of joint inversion of seismic AVA and CSEM data for estimating gas saturation under field conditions. In the following, we first briefly describe seismic and CSEM data used in this study and then compare the inversion results with the borehole logs. Detailed information on this site is given by Hoversten et al. (2006).

Seismic AVA data

Many types of geophysical surveys have been conducted over the past 30 years. For this study, we chose marine seismic AVA and CSEM data near well 31/2–1. Seismic AVA data were collected from common-depth-point (CDP) locations within 50 m of EM receivers sitting on the seafloor. At each CMP location, there are six incident angles (7.2°, 13.5°, 19.8°, 25.6°, 31.1°, and 36.3°). Figure 8 shows the prestack NMO-corrected data at CMP 1147, which is near the marine CSEM receiver Rx16. From the figure, we see a strong reflector near 1500 ms that may correspond to the top of the gas reservoir. Similarly, we can determine approximately the bottom of the reservoir, which is around 1800 ms. Consequently, we chose the prestacked data between 1418 and 1816 ms for seismic AVA data inversion. Angle-dependent wavelets were also derived by matching seismic data at a well 1.5 km away from this site.

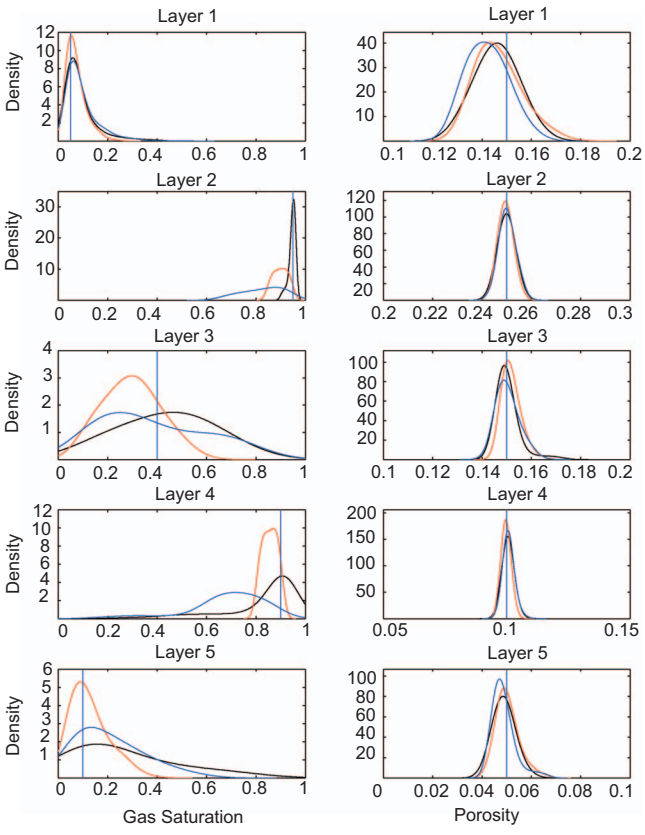

Figure 7. A comparison between the estimated PDFs of gas saturation and porosity using seismic AVA and CSEM data when oil concentrations are given (black), uniformly distributed on (0,0.1) (red), and uniformly distributed on (0,0.3) (blue).

Marine CSEM data

Marine CSEM surveys measure the EM responses of electrical resistivity in the entire half-space under the ocean surface that includes seawater, overburden, gas reservoir, and bedrock. The recorded CSEM data are the in-phase and out-of-phase electrical fields collected at three frequencies (0.25, 0.75, and 1.25 Hz). To be consistent with the seismic AVA data, we use the CSEM data obtained from receiver Rx16 for eight transmitters; source-receiver distances are 775, 1700, 2500, 3300, 4100, 4900, 5700, and 6500 m, respectively. The relative errors of those CSEM data are estimated to be 10%.

Prior distribution

We use different methods to determine the prior distributions of unknown parameters in the potential reservoir and in the zones outside the reservoir. For the unknown parameters in the zones outside of the reservoir (i.e., seismic bulk and shear moduli, density, and the overburden and bedrock conductivity), we assume they are distributed uniformly between 70% and 130% of their corresponding borehole logs collected from well 31/2–1. For the unknown parameters in the reservoir (i.e., fluid saturation and porosity), we assume they are distributed uniformly within given bounds.

We first determine reference values for water and gas saturation. According to information obtained from the nearby borehole logs,

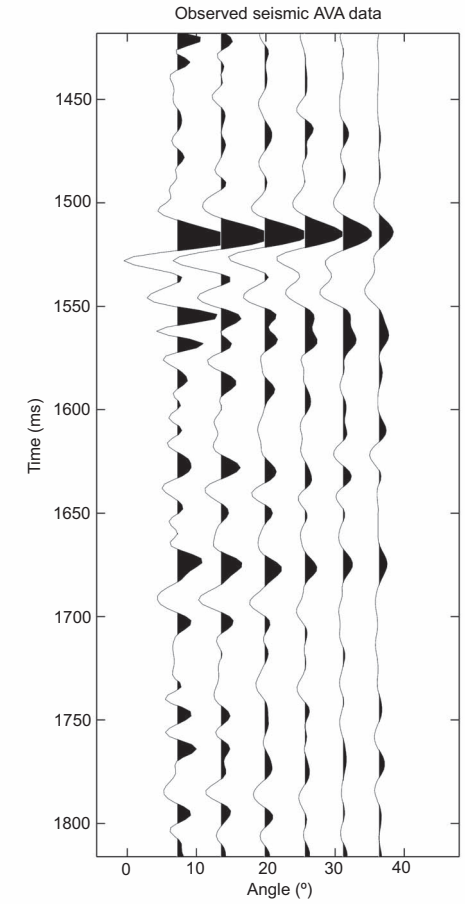

Figure 8. Prestacked NMO corrected seismic AVA data at CMP 1147 of the Troll Site.

we assume that the values for water saturation range from zero to one and the values for gas saturation range from one to zero from the top to the base of the reservoir. The bounds for water and gas saturation are the reference values ±0.3. The lower bounds of oil saturation are zero for all the layers, and the upper bound is 0.1 for depths less than 1544.5 m. Below 1544.5 m, the upper bounds of oil saturation linearly decrease from 0.7 to 0.1 at the base of the reservoir to allow oil where it was originally present.

Inversion of seismic AVA data

For inversion of seismic data, we divide the potential reservoir into 16 layers with a thickness of 20 m and consider porosity, water saturation, and gas saturation in each layer to be unknown parameters. To account for uncertainty in the time-depth function that provides the time window for the seismic AVA data, we also include five 20-m-thick layers above the reservoir and one 20-m-thick layer below the reservoir.

Figure 9 compares the inversion results using seismic AVA data with the borehole logs collected from well 31/2–1. The seismic AVA data provide good estimates of water saturation for layers 1–6, where water saturation is low. Because we only allow oil saturation to vary between 0.0 and 0.1, we obtain good estimates of gas saturation. However, for layers 7–13, inversion of seismic AVA data only provides poor estimates of water saturation. This is because seismic data have low sensitivity to variations in water saturation from 0.3–0.8, as found by Hoversten et al. (2006).

Joint inversion of seismic AVA and CSEM data

To invert seismic AVA and CSEM data jointly, we need to account for the effects of electrical conductivity of the overburden above the reservoir. In this study, we divide the overburden (including seawater) into 13 layers according to the resistivity logs collected from well 31/2–1 and consider the electrical conductivity in each of those layers as an unknown parameter. Figure 10 shows the prior bounds and initial values of the overburden electrical conductivity derived from well 31/2–1. We assume that the unknown overburden conductivity parameters are distributed uniformly in the given ranges.

Figure 11 shows the inversion results using both seismic AVA and CSEM data. For layers 1–6, the joint inversion provides estimates of water and gas saturation that are as close to borehole logs as the previous inversion. For layers 7–13, the joint inversion provides slightly better estimates of water saturation than those obtained from inversion of seismic data alone, but uncertainty in both estimates is large. Figure 12 from the top to the bottom compares the estimated PDFs of water and gas saturation for layers 7–12 using seismic data alone (black lines) and using both seismic and CSEM data (red lines). The blue lines show the results from the nearby borehole. Comparing the estimated modes with the borehole logs, we see that the joint inversion is better. Table 5 shows the rms of the differences

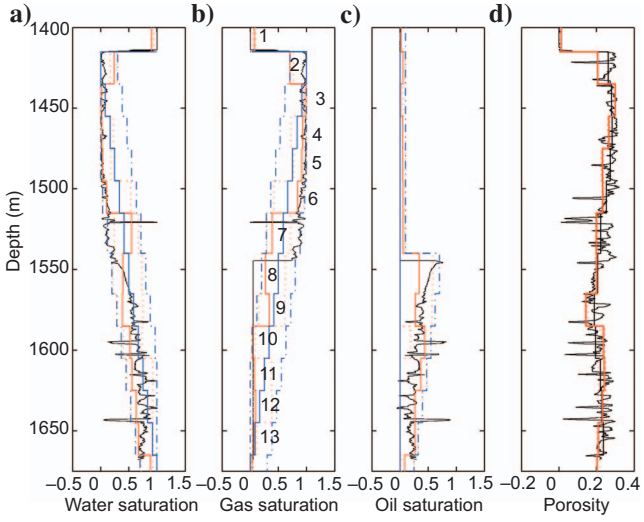

Figure 9. Estimated (a) water, (b) gas, (c) oil saturation, and (d) porosity using seismic AVA data alone. From (a) to (c) red lines show the modes of estimated marginal PDFs, the red dotted lines show the 95% predictive intervals, the black lines show borehole logs, and the blue lines show the prior distribution of unknown parameters. In (d) Red lines show the modes of estimated porosity PDFs, and the straight black lines show the blocked average of porosity.

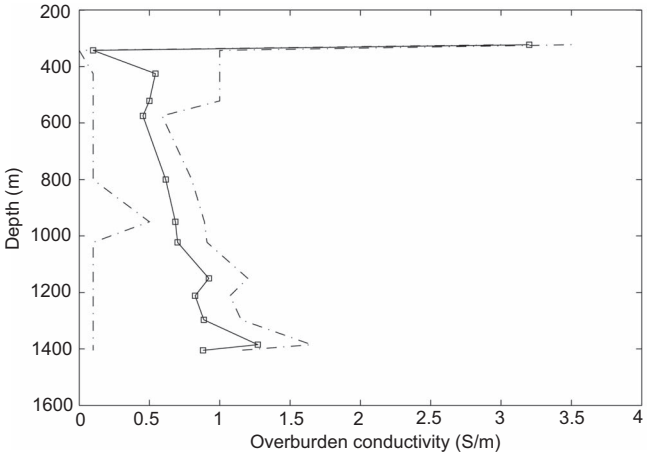

Figure 10. Prior bounds of the overburden electrical conductivity derived from borehole logs at well 31/2–1, where the solid lines show the initial values and the dash lines show the lower and upper bounds of the overburden conductivity.

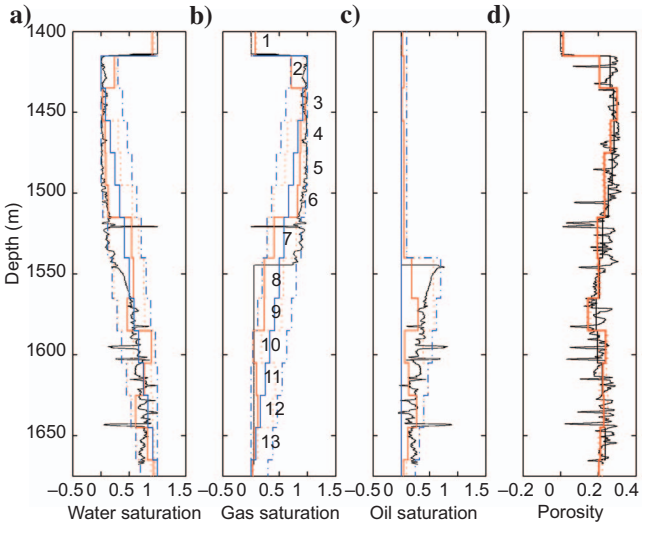

Figure 11. Estimated (a) water, (b) gas, (c) oil saturation, and (d) porosity using seismic AVA and CSEM data. From (a) to (c) red lines show the modes of estimated marginal PDFs, the red dotted lines show the 95% predictive intervals, the black lines show borehole logs, and the blue lines show the prior distribution of unknown parameters. In (d) Red lines show the modes of estimated porosity PDFs, and the straight black lines show the blocked average of porosity.

between the averaged well-log values and the estimated values (modes) from the Troll data sets. The joint inversion is slightly better.

Data misfit

To show how the estimated model (modes) fits the data, we compare the seismic AVA and CSEM responses of the estimated model with the corresponding seismic AVA and CSEM data. Figure 13 compares the in-phase and out-of-phase electrical fields of the estimated model with the CSEM data at three frequencies over eight offsets. The estimated model fits the electrical field at frequency 0.25 Hz well. However, for high frequencies (0.75 and 1.25 Hz), the fit is not good when offsets are larger than 3500 m. The misfit for large offsets at high frequencies could have many different causes. One possible reason for the misfit is the assumption of a layered reservoir model. The higher-frequency CSEM data typically have higher resolution; therefore, the 3D localized features of the gas reservoir affect the CSEM data.

Figure 14 shows the seismic AVA data misfit for the models obtained from the joint inversion of seismic and EM data. We see that joint inversion fits the seismic data well.

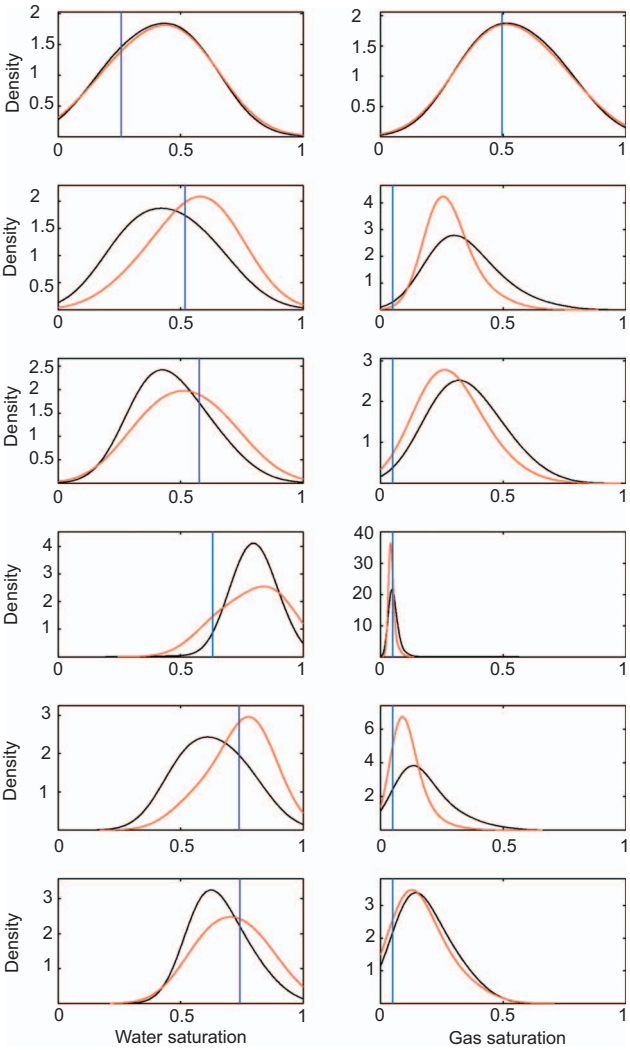

Figure 12. Comparison between the estimated water and gas saturation using seismic AVA data alone (black) and using both seismic AVA and CSEM data (red) from layers 7–12.

Table 5. The rms of the differences between the averaged well-log values and the estimated modes for Troll data sets.

	Water saturation	Gas saturation	Oil saturation	Porosity
Seismic AVA data only	0.1877	0.1760	0.0965	0.0431
Seismic AVA and marine CSEM data	0.1398	0.1650	0.1112	0.0442

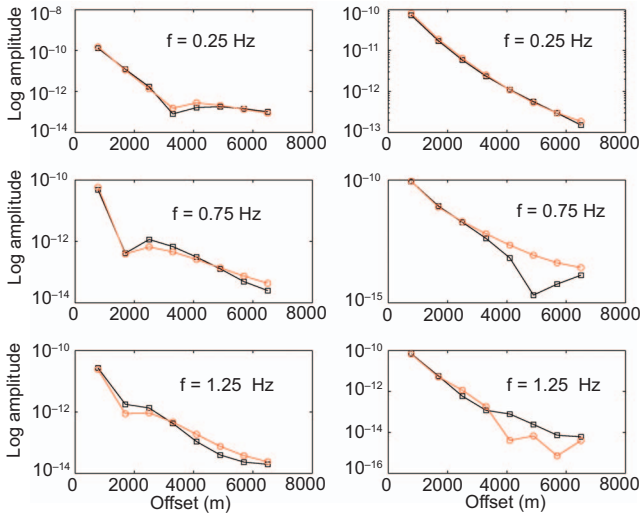

Figure 13. Comparison between the observed (black) and the calculated (red) inphase (left) and out-of-phase (right) of the electrical field using the modes of the estimated PDFs obtained from joint inversion of seismic AVA and CSEM data.

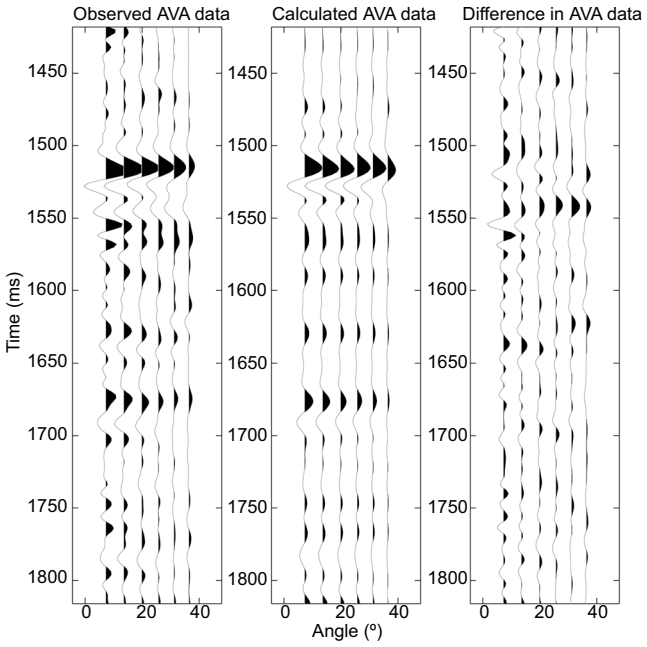

Figure 14. Comparison between the observed and calculated seismic AVA data using parameters obtained from joint inversion of seismic AVA and CSEM data.

CONCLUSIONS

We develop a Bayesian model to estimate gas saturation using marine seismic AVA and CSEM, and we demonstrate the capability of the model to solve nonlinear and nonunique inverse problems using a five-layer synthetic reservoir model. Unlike deterministic inverse methods that typically provide single value estimation and have difficulty in finding the global solutions, the stochastic methods draw many samples of unknown parameters from the joint posterior distribution function. The obtained samples allow us to evaluate the means, variances, modes, predictive intervals, and marginal PDFs of unknown parameters, all of which are useful for quantifying the uncertainty associated with inversion.

We also demonstrate the advantages of joint inversion over individual inversion of seismic AVA and CSEM data for gas saturation estimation using the five-layer model. Using seismic AVA data alone, even with high resolution, it is difficult to distinguish high or low gas concentration in deep layers because seismic properties are not sensitive to variations in gas concentration. With the inclusion of CSEM data, uncertainty in gas saturation estimation decreases, and the ability to identify high gas concentration in deep layers is enhanced. The improvement is affected by uncertainty in the overburden and bedrock electrical conductivity and by prior knowledge of oil concentration. The effects of uncertainty in the overburden and bedrock conductivity is less than those of prior knowledge on oil concentration. It is possible, if we increase incident angles of seismic AVA data (e.g., up to 40°), prior knowledge about oil concentration may have less effect on gas saturation estimation. Other factors may also affect the joint inversion, such as uncertainty in the estimates of seismic waveforms, rock-physics models, and approximations of 1D reservoir models, which will be explored in later studies.

Finally, we apply the Bayesian model to a data set collected from the Troll site. Although seismic waveforms and rock-physics models are estimated from borehole logs with uncertainty and both seismic AVA and CSEM data are 3D data, a comparison between the results using seismic AVA data alone and the results using both seismic AVA and CSEM data shows that joint inversion of seismic and CSEM data provides better estimates of gas saturation. The benefits of combining seismic AVA and CSEM data are more striking in synthetic tests than in the field data example. Part of the difference is almost certainly a result of the large number of unknown noise sources inherent in the field data. These may include noise in the estimated angle-dependent wavelets and the possible presence of correlated non-Gaussian noise in both seismic AVA and CSEM data sets. The saturation and porosity logs, assumed to be ground truth, can also be in error. In addition, the 1D model may not accurately represent the actual earth. This is more likely to be a problem for the CSEM data, which has a larger spatial footprint, than for the seismic AVA modeling, although the assumption that all multiples have been removed and that true relative amplitudes have been recovered in the seismic data may also not be strictly valid. In any case, we believe our synthetic examples provide sufficient evidence of the improvements possible when seismic AVA and CSEM data are combined so as to induce others to improve on our efforts with field data.

ACKNOWLEDGMENTS

The work is funded by the Research Partnership to Secure Energy for America (RPSEA) and the U. S. Department of Energy under contract DE-AC03-76SF00098.

REFERENCES

Aki, K., and P. G. Richards, 1980, Quantitative seismology: Theory and methods: W. H. Freeman & Co.

Archie, G. E., 1942, The electrical resistivity log as an aid in determining some reservoir characteristics: Transactions of the American Institute of Mechanical Engineers, 146, 54–62.

Batzle, M., and Z. Wang, 1992, Seismic properties of pore fluids: Geophysics, **57**, 1396–1408.

Besag, J., 2001, Markov chain Monte Carlo for statistical inference: Center for Statistics and the Social Sciences, University of Washington report 9, 1–67.

Bosch, M., 1999, Lithologic tomography: From plural geophysical data to lithology estimation: Journal of Geophysical Research, **104**, 749–766.

———, 2004, The optimization approach to lithological tomography: Combining seismic data and petrophysics for porosity prediction: Geophysics, **69**, 1272–1282.

Buland, A., and H. Omre, 2003a, Bayesian linearized AVO inversion: Geophysics, **68**, 185–198.

———, 2003b, Bayesian wavelet estimation from seismic and well data: Geophysics, **68**, 2000–2009.

———, 2003c, Joint AVO inversion, wavelet estimation and noise-level estimation using a spatially coupled hierarchical Bayesian model: Geophysical Prospecting, **51**, 531–550.

Castagna, J. P., 1993, AVO analysis — Tutorial and review, *in* J. P. Castagna and M. M. Backus, eds., Offset-dependent reflectivity — Theory and practice of AVO analysis: Investigations in Geophysics 8, SEG, 3–36.

Debski, W., and A. Tarantola, 1995, Information on elastic parameters obtained from the amplitudes of reflected waves: Geophysics, **60**, 1426–1436.

Dvorkin, J., and A. Nur, 1996, Elasticity of high-porosity sandstones: Theory for two North Sea datasets: Geophysics, **61**, 1363–1370.

Ellingsrud, S., T. Eidesmo, S. Johansen, M. C. Sinha, L. M. MacGregor, and S. Constable, 2002, Remote sensing of hydrocarbon layers by seabed logging (SBL): Results from a cruise offshore Angola: The Leading Edge, **21**, 972–982.

Gassmann, F., 1951, Elastic waves through a packing of spheres: Geophysics, **16**, 673–685.

Gelfand, A. E., and A., F. M. Smith, 1990, Sampling based approaches to calculating marginal densities: Journal of the American Statistical Association, **85**, 398–409.

Geman, S., and D. Geman, 1984, Stochastic relaxation, Gibbs distributions, and the Bayesian restoration of images: IEEE Transactions on Pattern Analysis and Machine Intelligence, **6**, 721–741.

Gilks, W., S. Richardson, and D. Spiegelhalter, 1996, Markov chain Monte Carlo in Practice: Chapman & Hall/CRC Press.

Hashin, Z., and S. Shtrikman, 1963, A variational approach to the elastic behavior of multiphase materials: Journal of the Mechanics and Physics of Solids, **11**, 127–140.

Hastings, W. K., 1970, Monte Carlo sampling methods using Markov chains and their applications: Biometrika, **57**, 97–109.

Hou, Z., Y. Rubin, M. Hoversten, D. Vasco, and J. Chen, 2006, Reservoir parameter identification using minimum relative entropy-based Bayesian inversion of seismic AVA and marine CSEM data: Geophysics, **71**, no. 6, O77–O88.

Hoversten, G., F. Cassassuce, E. Gasperikova, G. Newman, J. Chen, D. Vasco, Y. Rubin, and Z. Hou, 2006, Direct reservoir parameter estimation using joint inversion of marine seismic AVA and CSEM data: Geophysics, **71**, no. 3, C1–C13.

Hoversten, G. M., R. Gritto, J. Washbourne, and T. Daley, 2003, Pressure and fluid saturation prediction in a multicomponent reservoir using combined seismic and electromagnetic imaging: Geophysics, **68**, 1580–1591.

Malinverno, A., 2002, Parsimonious Bayesian Markov chain Monte Carlo inversion in a nonlinear geophysical problem: Geophysical Journal International, **151**, 675–688.

Mavko, G., T. Mukerji, and J. Dvorkin, 1998, The rock-physics handbook: Tools for seismic analysis in porous media: Cambridge University Press.

Metropolis, N., A. W. Rosenbluth, M. N. Rosenbluth, A. H. Teller, and E. Teller, 1953, Equations of state calculations by fast computing machines: Journal of Chemical Physics, **21**, 1087–1092.

Mindlin, R. D., 1949, Compliance of elastic bodies in contact: Transactions of American Society of Mechanical Engineers, **71**, A–259.

Neal, R. M., 2003, Slice sampling: The Annuals Statistics, **31**, 705–767.

Plessix, R., and J. Bork, 2000, Quantitative estimation of VTI parameters from AVA responses: Geophysical Prospecting, **48**, 87–108.